Multidimensional Conformational Free Energy Surface Exploration: Helical States of Ala_n and Aib_n Peptides

Yan Wang and Krzysztof Kuczera*

Departments of Chemistry and Biochemistry, University of Kansas, 2010 Malott Hall, Lawrence, Kansas 66045

Received: December 9, 1996; In Final Form: March 5, 1997[⊗]

A new multidimensional thermodynamic integration method is applied to investigate free energy surfaces of alanine (Ala) and α-methylalanine (Aib) homopeptides in the helical region. In this approach a single molecular dynamics simulation with all ϕ and ψ dihedrals kept fixed yields the free energy gradient with respect to all the fixed conformational coordinates. For regular structures of model peptides $(Ala)_n$ and $(Aib)_n$, where $n =$ 6, 8, 10 and Aib is α-methylalanine in vacuum, free energy maps in $\phi-\psi$ space are calculated and used to roughly locate free energy minima. For $(Ala)_n$, α-helical minima are found for $n = 6$, 8, 10 and a π-helical minimum exists for $n = 10$, while all studied $(Aib)_n$ peptides have stable α- and 3_{10}-helical states. The locations of the free energy minima are further refined by the novel procedure of free energy optimization by steepest descent down the gradient, leading to structures in excellent agreement with experimental data. The stability of the minima with respect to deformations is studied by analysis of second derivatives of the free energy surface. Analysis of free energy components and molecular structures uncovers the molecular mechanism for the propensity of Aib peptides for the 3_{10}-helix structure in the interplay between the quality and quantity of hydrogen bonds. The $(Ala)_{10}$ α-helix is favored over the 3_{10}-helix by all energy terms, exhibiting lower internal strain, lower van der Waals repulsion, and more favorable electrostatic interactions. Although the 3_{10}-helix has one more hydrogen bond, in $(Ala)_n$ each individual helical hydrogen bond is weaker in the 3_{10}-helix than in the α-helix. In $(Aib)_n$ peptides the added bulk of the α-methyls subtly deforms the helices, inducing larger internal strain and larger van der Waals repulsion than in corresponding $(Ala)_n$ structures and making the $(Aib)_n$ hydrogen bond geometry better in the 3_{10}- than in the α-helix. The synergistic effect of greater number of hydrogen bonds and improved interactions within each bond strongly stabilizes the $(Aib)_n$ 3_{10}-helix, making it the favored structure for short peptides.

I. Introduction

Conformational free energy simulations are being widely used in simulations of complex molecular systems.[1−3] Calculating free energy differences between molecular states is valuable because they are observable thermodynamic quantities, related to equilibrium constants and rate constants of processes. When the system is driven along a reaction path, free energy simulations enable enhanced conformational sampling and exploring structural regions separated by barriers that are impossible to overcome in direct, unconstrained simulations of feasible length.[4,5] Additionally, analysis of free energy components yields valuable insight into the microscopic forces involved in the studied processes.[6−8]

Conformational changes in molecular systems occur without modifications of chemical structure and include molecular association, rotational isomerism, and more complex structural transitions. Free energy simulations of such processes mainly employ four approaches—direct sampling, umbrella sampling, thermodynamic perturbation, and thermodynamic integration.[1−3,9,10] A number of structural changes have been studied in this way, including torsions in *n*-butane (see refs 8 and 11 for recent works) and peptide side chains,[9,12] as well as aggregation of methane[10] and a helix bundle protein in water[13] and the α-helix → 3_{10}-helix transition in model peptides.[14−16]

Recently, a new approach to conformational free energy simulations has been proposed—the CFTI method (for conformational free energy thermodynamic integration).[8] The CFTI method is based on the observation that it is possible to calculate the conformational free energy gradient with respect to an arbitrary number of conformational coordinates from a single simulation with all coordinates in the set kept fixed.[8] CFTI has a number of interesting properties. When simulations are performed with all "soft" degrees of freedom of the system kept fixed, free energy averages converge very quickly, effectively overcoming the conformational sampling problem. Further, the availability of the conformational gradient makes possible novel techniques of multidimensional conformational free energy surface exploration, including locating free energy minima by free energy optimization and analysis of structural stability based on second derivatives of the free energy. The subject of this work is the application of these techniques to studies of the conformational free energy surfaces of helical structures of model peptides—$(Ala)_n$ and $(Aib)_n$, where $n = 6$, 8, 10 and Aib is α-methylalanine. Three types of helical conformations are expected to fall within the explored conformational region—α-, 3_{10}-, and π-helices.[17] The problems addressed are which types of helices form stable states for the studied systems and what are the intrinsic and relative stabilities of the different helical conformations as a function of peptide length and C_α substitution.

Alanine and α-methylalanine homopeptides serve as models of more general peptide and protein systems. Conformational studies of these models have important implications for our understanding of such phenomena as protein folding, conformational equilibria of flexible peptide drugs, thermodynamic stability of ordered structures of short peptides, and structural preferences of different amino acid residues.[5,14−16,18,19] The relative stability of the α-helix and 3_{10}-helix structures is also

* To whom correspondence should be addressed. Email: kuczera@tedybr.chem.ukans.edu.

[⊗] Abstract published in *Advance ACS Abstracts,* June 1, 1997.

S1089-5647(96)04027-8 CCC: $14.00

of specific interest because about 10% of residues in helical protein structures take on the 3_{10}-helix conformation.[20] The enhanced stability of the 3_{10}-helix in Aib-containing peptides is well-known, but the molecular mechanism responsible for this effect is still under discussion.[14,16,19,21] Our studies provide new types of information about the free energy surfaces of $(Ala)_n$ and $(Aib)_n$ peptides, which yield novel insights into this question.

Preliminary work on this project has been described in the paper presenting the CFTI method.[8] In that work free energy gradient maps of $(Ala)_{10}$ and $(Aib)_{10}$ were calculated over a limited range of structures, the existence and rough location of the $(Ala)_{10}$ α-helix and $(Aib)_{10}$ α-helix and 3_{10}-helix free energy minima were determined, and estimates of the α-helix−3_{10}-helix free energy difference were obtained. In this work we wish to extend these studies by considering peptides of different length, over a wider range of conformations, as well as by applying new methods of free energy surface analysis. We start by generating extended free energy gradient maps for regular structures of $(Ala)_n$ and $(Aib)_n$ helices, with $n = 6$, 8, 10, for which the (ϕ,ψ) dihedral values are the same at each residue. These maps are used to roughly locate free energy minima and integrated to give corresponding free energy surfaces. The locations of the free energy minima are further refined by the novel procedure of free energy optimization by steepest descent down the gradient. The stability of the individual minima with respect to deformations is studied by analysis of second derivatives of the free energy surface. The relative free energies of the different stable states are evaluated by integrating the free energy gradient along paths connecting the corresponding structures. Additionally, decomposition of the overall free energy change into components from different effects, coupled with structural analysis, is used to explain the molecular mechanism of the increased stability of the 3_{10}-helix state in Aib-containing peptides. The CFTI simulation results not only reproduce the well-known effects of decreased stability of shorter helices and propensity of Aib-containing peptides for the 3_{10}-helix but also enable the analysis of contributing effects. These results provide an illustration of the new types of information that may be obtained from the multidimensional CFTI approach.

A brief theoretical background is given in part II, Theoretical Background, applications of the CFTI method to study of the $(Ala)_n$ and $(Aib)_n$ free energy surfaces are given in parts III, Simulation Details, and IV, Results and Discussion, and the Conclusions are presented in part V.

II. Theoretical Background

Consider a molecular system of N atoms, e.g. a solute in a solvent or a macromolecule, with a separable Hamiltonian $H(p,q) = K(p) + U(q)$, where K is the kinetic and U the potential energy, q are the $3N$ Cartesian coordinates, and p are the $3N$ conjugate momenta. In the canonical ensemble of statistical mechanics, at the constant number of particles N, volume V, and temperature T, the probability distribution of $\rho(\xi)$ of a generalized conformational coordinate ξ is:[22,23]

$$\rho(\xi') = \int \mathrm{d}q\, \rho(q)\, \delta(\xi(q)-\xi') = \frac{1}{Z}\int \mathrm{d}q\, \mathrm{e}^{-\beta U(q)}\, \delta(\xi(q)-\xi') \tag{1}$$

$$Z = \int \mathrm{d}q\, \mathrm{e}^{-\beta U(q)}$$

where $\rho(q)$ is the canonical coordinate probability distribution, Z is the classical configurational integral, and $\beta = 1/kT$, where k is the Boltzmann constant. The probability distribution $\rho(\xi)$ may be related to a conformational free energy profile or potential of mean force $A(\xi) = -kT \ln \rho(\xi)$. The standard thermodynamic integration (TI) formula for the derivative of $A(\xi)$ is[8,23]

$$\frac{\partial A(\xi')}{\partial \xi'} = \langle -F(\xi') \rangle_{\xi'} \tag{2}$$

$$F(\xi') = -\frac{\partial U}{\partial \xi'} + \beta^{-1}\frac{\partial \ln |J|}{\partial \xi'} \tag{3}$$

According to eq 2, in the TI scheme the derivative of the conformational free energy with respect to the chosen coordinate ξ is calculated by performing simulations with fixed values of ξ and evaluating averages of the generalized force F. This force includes a derivative of the potential $\partial U/\partial \xi$ and a term involving the Jacobian J of the coordinate transformation between the coordinates q and a complete set of generalized coordinates which includes ξ and is due to the generally nonlinear nature of $\xi(q)$.[8,23]

Analogously to eqs 1 and 2, we can introduce the joint probability distribution of a set of conformational coordinates ξ_k, $k = 1, ..., m$ (ref 8)

$$\rho(\xi'_1,\xi'_2,...,\xi'_m) = \int \mathrm{d}q\, \rho(q) \prod_{k=1}^{m} \delta(\xi_k(q)-\xi'_i) \tag{4}$$

and show that the gradient of the free energy surface $A(\xi'_1,\xi'_2, ..., \xi'_m)$ with respect to the set of coordinates ξ_k is[8]

$$\frac{\partial A(\xi'_1,\xi'_2,...,\xi'_m)}{\partial \xi'_k} = \langle -F_k \rangle_{\xi'_i, i=1,...,m} \qquad k = 1, ..., m \tag{5}$$

$$F_k = -\frac{\partial U}{\partial \xi'_k} + \beta^{-1}\frac{\partial \ln |J|}{\partial \xi'_k} \tag{6}$$

That is, to calculate the derivatives $\partial A/\partial \xi_k$, $k = 1, ..., m$ of the conformational free energy with respect to the set of generalized coordinates ξ_k, we have to evaluate the averages of the set of generalized forces F_k over conformations with all coordinates ξ_k fixed.

The multidimensional entropy surface $S(\xi'_1,\xi'_2,...,\xi'_m)$ may be defined in the standard way:

$$A(\xi'_1,\xi'_2,...,\xi'_m) = \langle U(q) \rangle_{\xi'_i, i=1,...,m} - T\cdot S(\xi'_1,\xi'_2,...,\xi'_m) \tag{7}$$

Using the previously developed formalism (eq 22 from Appendix A in ref 8, with $X = U(q)$), the formula for the gradient of S may be derived

$$T\frac{\partial S(\xi'_1,\xi'_2,...,\xi'_m)}{\partial \xi_k} = \frac{\partial}{\partial \xi_k}\langle U(q) \rangle_{\xi'_i, i=1,...,m} - \frac{\partial A_c(\xi)}{\partial \xi_k} \tag{8}$$

$$= -\beta[\langle U(q) F_k \rangle_{\xi'_i, i=1,...,m} - \langle U(q) \rangle_{\xi'_i, i=1,...,m} \langle F_k \rangle_{\xi'_i, i=1,...,m}] + \beta^{-1}\left\langle \frac{\partial \ln |J|}{\partial \xi'_k} \right\rangle_{\xi'_i, i=1,...,m} \qquad k = 1, ..., m$$

which is analogous to the one-dimensional formula[8] and where again terms involving the Jacobian appear due to the generally nonlinear nature of the $\xi_k(q)$.

The availability of the conformational free energy gradient with respect to a chosen set of coordinates is a starting point for exploration of multidimensional free energy surfaces. It enables complete local characterization of the free energy surface and opens the way to location and characterization of stationary

points and calculation of minimum free energy paths. Calculations of the free energy gradient carry very little computational overhead compared to evaluating a single derivative, since the most costly terms—the potential energy and its Cartesian gradient—are known in advance in standard computer simulations.[8] Decompositions of the free energy into energetic and entropic terms is possible—see eq 7 and ref 8. Additionally, because of the linear dependence of the free energy gradient on the potential, the free energy changes between states may be decomposed into contributions from the different terms in the potential—internal strain, electrostatic, van der Waals—as well as contributions from different parts of the system—solute, solvent, or individual chemical groups.[8] The latter decompositions are not rigorous but provide useful insight into the molecular effects contributing to the observed phenomena.[7,8,24] Taken together, the computational efficiency, analytical capability, and general applicability of the thermodynamic integration conformational free energy simulation approach make it a powerful tool in studies of conformational processes of flexible molecules.

III. Simulation Details

The Molecular Model. The new CHARMM Version 22 all-hydrogen model was used to describe the potential energy of the simulated systems.[25−27] The peptides studied here are acetylated at the N terminus and amidated at the C terminus; their chemical formulae are $(Ala)_n$, $CH_3CO-(Ala)_n-CONH_2$, and $(Aib)_n$, $CH_3CO-(Aib)_n-CONH_2$, where $n = 6$, 8, 10 and Aib is α-methylalanine. The $(Ala)_{10}$ system consists of 109 atoms and has 248 degrees of freedom after application of SHAKE constraints to bonds involving hydrogen atoms and fixing all ϕ and ψ backbone dihedrals, while $(Aib)_{10}$ consists of 139 atoms and has 318 degrees of freedom under the same conditions. The parameters and charges for both Aib methyl groups were taken to be identical to the standard Ala methyl.[27,26] In accord with CHARMM 22 all-atom force field conventions,[26,27] the Aib α-methyl group had the standard CHARMM methyl charges of $-0.27e$ at the carbon and $0.09e$ at the hydrogens. The charge on C_α was adjusted from the Ala value of $0.07e$ to $0.16e$ so as to maintain electrical neutrality of the new residue. In energy calculations an atom-based 12.0 Å nonbonded cutoff distance was employed, with a switching function between 10.0 and 12.0 Å for van der Waals terms and a shift function at 12.0 Å for electrostatics, in order to eliminate discontinuities due to the cutoff. The formulae used are given in eqs 15 and 16 of ref 25; a discussion of different cutoff schemes is available.[28] Full nonbonded interactions were calculated for all atoms separated by three or more chemical bonds.

Free Energy Gradient Maps. The peptides were simulated in vacuum, with all $2(n-1)$ ϕ and ψ dihedrals fixed at constant values:

$$\phi_i = \phi, \quad i = 2,...,n; \quad \psi_i = \psi, \quad i = 1,...,n-1$$

where i is the residue number. The conformations studied thus correspond to regular structures with identical conformations of each residue and may be identified by the pair of values (ϕ,ψ). For each of the $(Ala)_n$ and $(Aib)_n$ peptides, $n = 6$, 8, 10, simulations were performed in vacuum, at 221 points on a square grid with 3° spacing, for ϕ varying from −81° to −45° and ψ from −14° to −62°. The idealized right-handed π-helix, α-helix, and 3_{10}-helix conformations are expected to fall into this region. At each point the system coordinates were generated from model geometric parameters. A short energy minimization was followed by random velocity assignment, a 20 ps equilibration period of molecular dynamics with velocity rescaling to bring the temperature close to 300 K and a 40 ps trajectory generation phase at 300 K. The ϕ and ψ dihedrals were kept fixed at the required values during the minimization equilibration and dynamics using the holonomic constraint method of Tobias and Brooks.[8,29,30]

Simulations of n-residue peptides involved $2(n-1)$ dihedral constraints and yielded $2(n-1)$ components of the free energy gradient with respect to the individual ϕ and ψ according to eq 5: $\nabla A = (\partial A/\partial\phi_2,...,\partial A/\partial\phi_n,\partial A/\partial\psi_1,...,\partial A/\partial\psi_{n-1})$ at all explored points. To facilitate the analysis of this data the free energy gradient components corresponding to all ϕ and all ψ were added up to give

$$\frac{\partial A}{\partial \phi} = \sum_{i=2}^{n} \frac{\partial A}{\partial \phi_i}; \quad \frac{\partial A}{\partial \psi} = \sum_{i=1}^{n-1} \frac{\partial A}{\partial \psi_i}$$

This procedure leads to an effective two-dimensional (2D) free energy surface describing concerted conformational transitions between regular structures of the studied peptides. Reducing the dimensionality of the free energy surface from $2(n-1)$ to 2 allows for a more facile analysis of results. By following only concerted changes in the ϕ and ψ, we obtain only a partial description of the $2(n-1)$-dimensional conformational space. However, the complete $2(n-1)$-dimensional gradient is available at all explored points, enabling a more in-depth characterization of the visited parts of the surface if necessary.

The free energy surfaces were obtained by integrating the two-dimensional gradients starting out from a point in the vicinity of the lowest-lying free energy minimum, so that all free energy values would be positive. The apparent force terms involving $\ln|J|$ in eqs 3 and 6 were neglected in our calculations based on trial evaluations for $(Ala)_{10}$.[8]

Free Energy Optimization. Free energy optimization was performed by the steepest descent method.[31,32] In our implementation, free energy optimization consists of a sequence of steps, each involving evaluation of the free energy gradient ∇A from a simulation with all ϕ and ψ fixed followed by an adjustment of the dihedrals by a small step along $-\nabla A$. The length of the step is determined by estimating diagonal elements of the matrix of free energy second derivatives from gradient values at the current and previous step. This procedure is carried out until the the norm of ∇A falls to values comparable with its statistical error. The fact that this method converges to a stationary point on the free energy surface is confirmed by verifying that all gradient components change sign in this region, based on the full $2(n-1)$-dimensional gradients on surrounding grid points of the gradient map. Optimization by steepest descent is not the most efficient, suffering from well-known drawbacks.[31,32] Typical optimizations in the two-dimensional space of regular structures took 5−10 steps when starting from a grid point of low gradient identified from the free energy maps. More efficient methods are being developed.

The optimization method works equally well on the reduced two-dimensional free energy surfaces of regular structures and on the full $2(n-1)$-dimensional surfaces.

Numerical Second Derivatives. The free energy second derivative matrix $H_{ij} = \partial^2 A/(\partial\xi_i\,\partial\xi_j)$ was evaluated numerically on the two-dimensional free energy surface (ϕ,ψ) of regular helical structures. For each free energy minimum identified, the free energy gradients at the four surrounding grid points were used to estimate the elements of H_{ij}. The matrix was symmetrized and diagonalized using the Householder algorithm.[31]

Free Energy Profiles. Free energy profiles for the concerted α-helix → 3_{10}-helix transition were calculated for the studied peptides. Each profile simulation involved performing free energy gradient calculations for 15 equally spaced points along a straight line connecting the α-helix and 3_{10}-helix states in the reduced 2D (ϕ,ψ) space and integrating the gradient along this line. At each point the same protocol as for the map generation was followed—generation of model structure and energy optimization, 20 ps equilibration, and 40 ps trajectory generation at 300 K with fixed values of all ϕ and ψ dihedrals. For $(Ala)_n$ systems, for which no minima in the 3_{10}-helix region were found, the paths connected the minima to the idealized 3_{10}-helix structure at (ϕ,ψ) = (−60°,−29°). For $(Aib)_n$ the path connected the α-helix and 3_{10}-helix minima.

Error Analysis. The basic quantities—free energy and entropy gradient components—were evaluated from trajectory averages, as in eqs 5 and 7. Statistical errors of these quantities were calculated as standard deviations of the mean of subaverages obtained by dividing the data into 20 contiguous blocks. Magnitudes of individual gradient components ($\partial A/\partial\phi_i$), ($\partial A/\partial\psi_i$) in the studied conformational regions fell in the 1−20 kcal/(mol rad) range, with statistical errors in the range of 0.1−0.4 kcal/(mol rad) and a general tendency for constant relative error of about 3−5%. The aggregate contributions ($\partial A/\partial\phi$) and ($\partial A/\partial\psi$) defined in the Free Energy Gradient Maps ranged from 1 to 120 kcal/(mol rad) for $n = 10$, and between 1 and 60 kcal/(mol rad) for $n = 6$ (see Figure 1). The errors in these quantities were in the 0.2−0.9 kcal/(mol rad) range for $n = 10$ and 0.2−0.5 kcal/(mol rad) for $n = 6$.

Errors of the profile line integrals and second derivative matrix elements were determined directly from gradient statistical errors by standard error propagation.[33] Values of errors for overall free energy changes ΔA and electrostatic and van der Waals components presented in Table 3 were 0.04−0.08 kcal/mol, while errors of the internal strain were below 0.01 kcal/mol.

Errors of the numerical second derivative matrix elements were determined from gradient statistical errors by error propagation. Errors in the second derivative matrix eigenvalues were determined from errors of matrix elements by error propagation based on the analytical formula for eigenvalues of a two-dimensional matrix.

Programs and Computers. The molecular dynamics simulations described here were performed using the program CHARMM (Version 22),[25] which has been extended and modified by the authors to implement the multidimensional CFTI method.[8] The computers used were IBM RS/6000 workstations at the Departments of Chemistry and Biochemistry of the University of Kansas at Lawrence, the Molecular Graphics and Modeling Laboratory and the Kansas Institute for Theoretical and Computational Science. One point of the decapeptide vacuum free energy gradient maps, involving 60 ps of molecular dynamics, took about 1 h of CPU time on an RS/6000-550.

IV. Results and Discussion

Free Energy Gradient Maps. Free energy gradient maps of $(Ala)_n$ and $(Aib)_n$ systems with $n = 6$, 8, 10 and free energy surfaces obtained from their integration are presented in Figures 1 and 2. The $(Ala)_{10}$ results (Figures 1a and 2a) indicate the presence of two minima—the α-helix, close to (ϕ,ψ) = (−66°,−41°), and the π-helix, close to (−75°,−56°). For $(Ala)_8$ and $(Ala)_6$ only the α-helix minimum is well defined (Figures 1b,c and 2b,c). A trough on the free energy surface is present in the π-helix region for these molecules, but free energy profiles along this trough do not display a minimum. The $(Aib)_n$ free energy gradient maps and corresponding surfaces (Figures 1d−f and 2d−f) indicate that for these systems minima corresponding to α and 3_{10} helices exist. Stable π-helix structures were not found in the explored region.

TABLE 1: Free Energy Minima for Regular $(Ala)_n$ and $(Aib)_n$ Helices in Vacuum

system	α-helix (ϕ,ψ)	3_{10}-helix (ϕ,ψ)
$(Ala)_n$		
$n = 10$	(−65.8°,−40.8°)	
$n = 8$	(−66.8°,−39.6°)	
$n = 6$	(−69.5°,−37.0°)	
exptl	(−65°,−41°)[a]	
$(Aib)_n$		
$n = 10$	(−56.8°,−51.6°)	(−53.2°,−29.7°)
$n = 8$	(−57.4°,−50.8°)	(−53.6°,−29.2°)
$n = 6$	(−58.2°,−48.8°)	(−53.8°,−28.8°)
exptl	(−57°,−50°)[b]	(−54°,−29°)[c]

[a] X-ray structures of protein α-helices.[35] [b] X-ray structures of Aib-peptide α-helices.[16] [c] X-ray structures of Aib-peptide 3_{10}-helices.[16]

The stable states occupy diagonal valleys, as is expected for helices where anticorrelated changes of ϕ and ψ on successive residues leave the hydrogen-bonding pattern relatively unchanged.[34]

Free Energy Optimization. Starting from grid points with low gradients in the stable state regions, free energy optimization was performed on the 2D (ϕ,ψ) surface of the regular structures, using the steepest descent method. This allowed precise location of free energy minima. The results are summarized in Table 1. For $(Ala)_n$ minima at (ϕ,ψ) = (−66°,−41°), (−67°,−40°), and (−70°,−37°) were found in the α-helix region for $n = 10$, 8, and 6, respectively. The results for the longer helices are in excellent agreement with the average values of (−65°,−41°) found in α-helices of protein crystals.[35] In $(Ala)_{10}$ a minimum in the π-helix region was also found, at (ϕ,ψ) = (−77°,−54°). Using the free energy surface from Figure 2a, the free energy of this state is about 13 kcal/mol above the α-helix. In the case of $(Aib)_n$ peptides, α-helical minima were at (−57°,−52°), (−57°,−51°), and (−58°,−49°) for $n = 10$, 8, and 6, respectively, in agreement with the values of ϕ between −57° and −55° and $\psi = -50°$ found in Aib homopeptide crystals.[36,37] The 3_{10}-helical minima of $(Aib)_n$ were located at (−53°,−30°) for $n = 10$ and (−54°,−29°) for both $n = 8$ and 6, again in accord with crystallographic results of giving ϕ in the −54° to −52° range and ψ from −31° to −28° for Aib homopeptides.[36,38,39]

Free energy minimization in the full $2(n - 1)$ dimensional space starting from the regular minima converged to similar irregular structures, with the main difference lying in some helix unwinding at the termini.

Stability of the Minima: Second Derivatives of the Free Energy. From the free energy gradient maps, the free energy second derivative matrix $H_{ij} = \partial^2 A/(\partial\xi_i\,\partial\xi_j)$ was evaluated numerically on the two-dimensional (2D) (ϕ,ψ) surface. The results are summarized in Table 2. The 2D H matrix eigenvalues were positive at the $(Ala)_n$ α-helical minima, the $(Ala)_{10}$ π-helix, and $(Aib)_n$ α-helical and 3_{10}-helical minima, confirming that these states are indeed free energy minima on the 2D (ϕ,ψ) surface of regular structures. The magnitudes of the eigenvalues provide information about the stability of the minimum free energy structures with respect to concerted deformations.

For the $(Ala)_{10}$ α-helix the H eigenvalues were 0.037 and 0.562 kcal/(mol deg^2), while the corresponding $(Aib)_{10}$ values were 0.046 and 0.541 kcal/(mol deg^2). The "hard modes" of the α-helices are thus of comparable stiffness in $(Ala)_{10}$ and $(Aib)_{10}$, but the "soft mode" is more rigid in the Aib system.

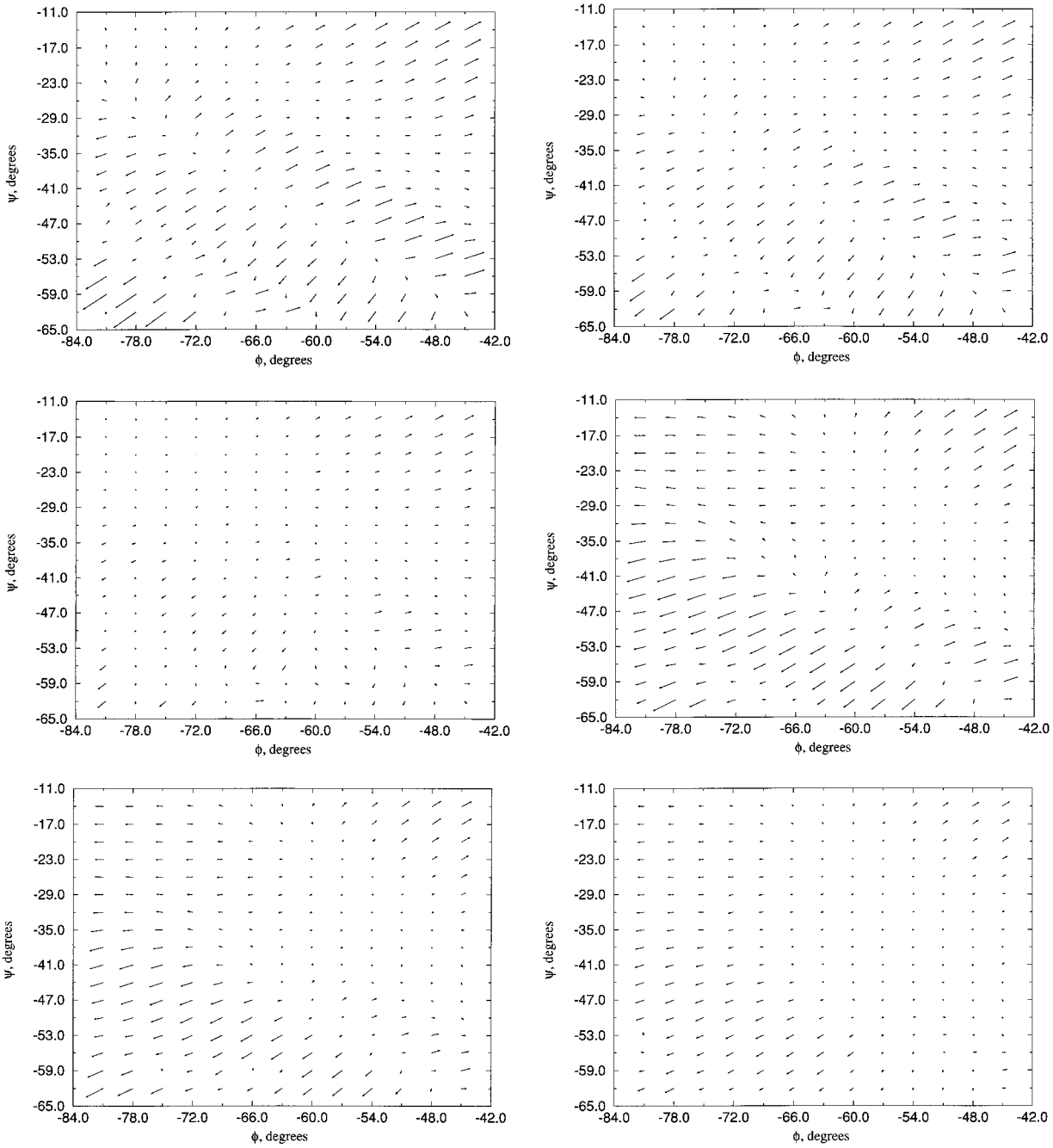

Figure 1. Reduced two-dimensional free energy gradient maps corresponding to regular helical structures of the studied peptides. Arrows indicate the direction of increasing conformational free energy ($\partial A/\partial\phi, \partial A/\partial\psi$): (a, top left) $(Ala)_{10}$, (b, top right) $(Ala)_8$, (c, middle left) $(Ala)_6$, (d, middle right) $(Aib)_{10}$, (e, bottom left) $(Aib)_8$, (f, bottom right) $(Aib)_6$.

The $(Aib)_{10}$ 3_{10}-helix was much easier to deform than the α-helix: the 3_{10}-helix eigenvalues were 0.030 and 0.118 kcal/(mol deg^2). For all structures the eigenvalues decreased with decreasing peptide length, as could intuitively be expected. For the $(Aib)_6$ α-helix the low eigenvalue 0.006 ± 0.002 kcal/(mol deg^2) was comparable to its statistical error, indicating that this structure is only marginally stable.

The H eigenvectors corresponding to the high and low eigenvalues define two modes of uniform helix deformations—the "hard" and "soft" modes, respectively. To understand the structural changes along these modes, the molecular dynamics average structures of the systems at grid points surrounding the minima were analyzed by calculating the helical rise, turn, and radius (see footnote in Table 4). On this basis it was determined that deformations along the soft mode, which involve anticorrelated changes of ϕ and ψ, correspond to variations of the helix radius only, with the rise and turn remaining approximately constant. This mode thus corresponds to a cylindrical breathing type of motion; it involves small variations of free energy because it leaves the hydrogen bond geometry approximately unchanged. Deformations of this type have been seen in previous simulations of peptide helices[34] and are also seen in distributions of α-helical structures in protein crystals.[35] The hard mode involves correlated changes in ϕ and ψ and corresponds to a concerted increase of rise and turn and decrease in helix radius. Motion in this direction approximately corresponds to the reaction coordinate for the $\alpha \rightarrow \pi$ and $\alpha \rightarrow 3_{10}$ transitions; its high energetic cost is due to hydrogen bond breaking.

The α-Helix → 3_{10}-Helix Free Energy Profiles. The free energy surfaces were further analyzed by calculation of free energy profiles along the α-helix → 3_{10}-helix path (see part III).

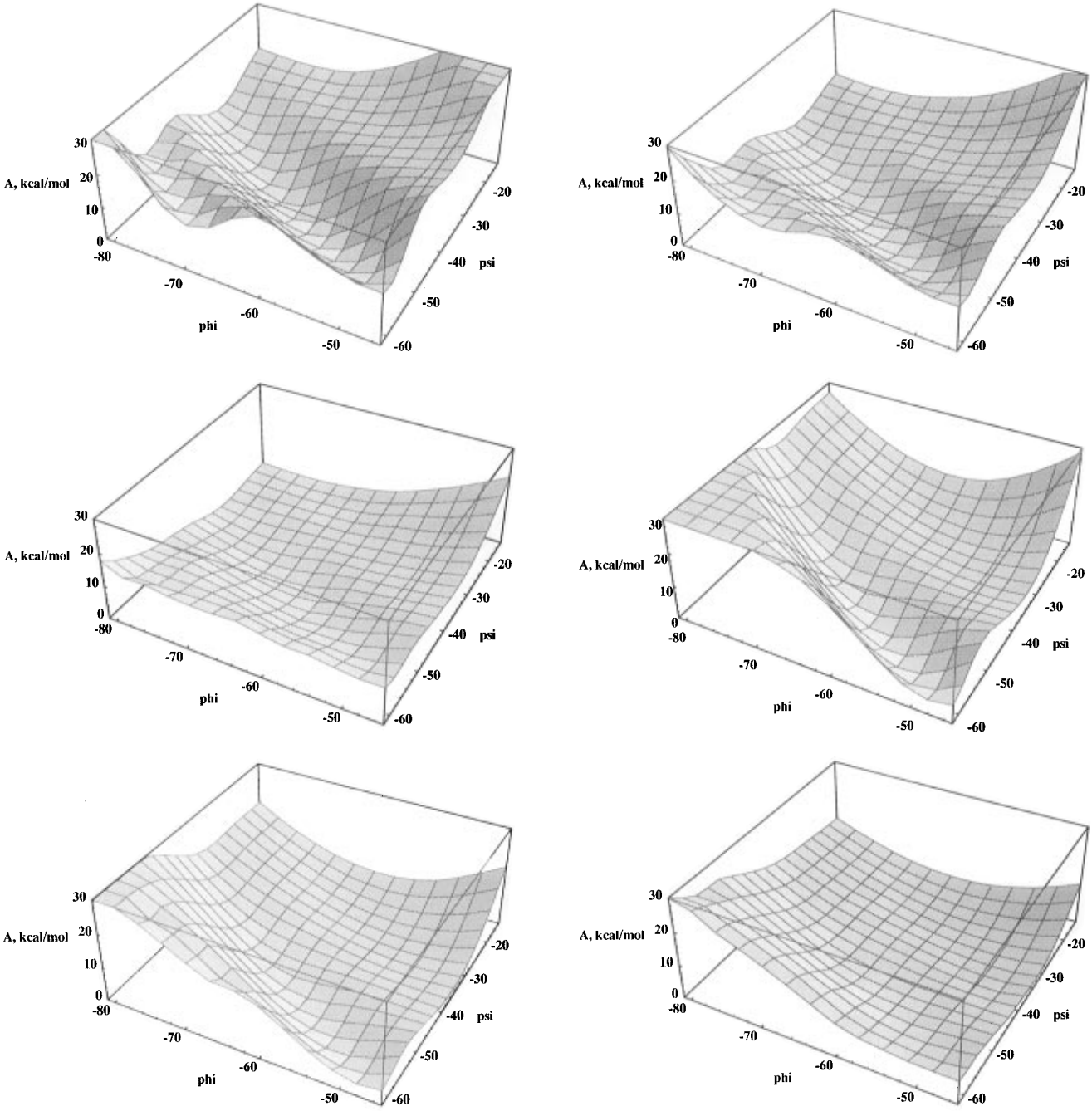

Figure 2. Reduced two-dimensional free energy maps A(ϕ,ψ) corresponding to regular helical structures of the studied peptides. Values obtained by integrating the gradient starting from the grid point closest to the most stable state: (a, top left) $(Ala)_{10}$, (b, top right) $(Ala)_8$, (c, middle left) $(Ala)_6$, (d, middle right) $(Aib)_{10}$, (e, bottom left) $(Aib)_8$, (f, bottom right) $(Aib)_6$.

TABLE 2: Deformation Constants for Regular $(Ala)_n$ and $(Aib)_n$ Helices in Vacuum[a]

	α-helix		3_{10}-helix	
system	*f*	*F*	*f*	*F*
$(Ala)_n$				
$n = 10$	0.037 ± 0.003	0.562 ± 0.003		
$n = 8$	0.025 ± 0.003	0.369 ± 0.003		
$n = 6$	0.017 ± 0.002	0.185 ± 0.002		
$(Aib)_n$				
$n = 10$	0.046 ± 0.003	0.541 ± 0.003	0.030 ± 0.002	0.118 ± 0.002
$n = 8$	0.031 ± 0.003	0.330 ± 0.003	0.016 ± 0.002	0.094 ± 0.002
$n = 6$	0.006 ± 0.002	0.117 ± 0.002	0.005 ± 0.001	0.057 ± 0.001

[a] Units: kcal/(mol deg^2). *f* and *F* are the low and high eigenvalues of the reduced 2D Hessian, respectively

The free energy profiles are described in Figure 3 and Table 3. To provide a better understanding of the overall free energy differences, decompositions are provided into energetic and entropic components, as well as into contributions from the different potential energy terms. Due to refinement of the location of the α-helix and 3_{10}-helix states in this work, the free energy differences calculated here differ slightly from the more approximate values given previously.[8]

The free energy difference between the α-helix and 3_{10}-helix decreases with decreasing peptide length for both $(Ala)_n$ and $(Aib)_n$ systems, as has been previously observed.[15,16,39,40] Since there are no minima in the 3_{10}-helix region of conformations for $(Ala)_n$, there is some ambiguity in structural and energetic comparisons between α-helix and 3_{10}-helix states. We have used a widely accepted model geometry of (ϕ,ψ) = ($-60°$,$-29°$) to represent the 3_{10}-helix structure, to facilitate comparisons between our results and previous simulations.[14,15]

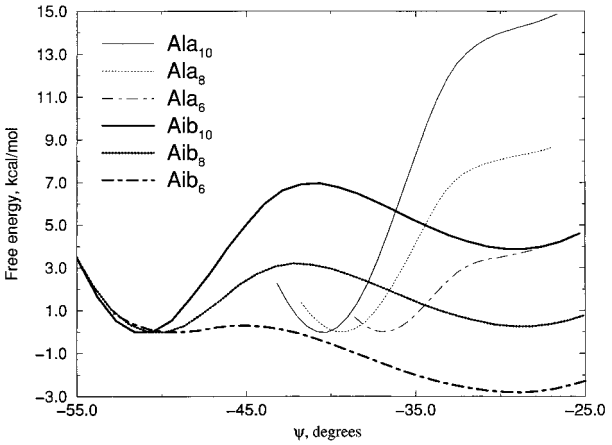

Figure 3. Free energy profiles for concerted α-helix → 3_{10}-helix transitions in the studied peptides. Free energy gradient integrated along straight line paths connecting minima to the idealized 3_{10}-helix structure at $(\phi,\psi) = (-60°,-29°)$ for $(Ala)_n$ and connecting the α-helix and 3_{10}-helix minima (see Table 1).

TABLE 3: Energetics of the Concerted α-Helix → 3_{10}-Helix Transition in $(Aib)_n$[a]

system	potential energy components[b]				energy−entropy components	
ΔA	total	int	elec	vdW	ΔU	$-T\Delta S$
			α → 3_{10}			
$(Ala)_{10}$	14.2	2.8	3.0	8.4	17.7 ± 0.4	−3.5 ± 0.4
$(Ala)_8$	8.3	1.9	−2.0	8.4	11.5 ± 0.3	−3.2 ± 0.3
$(Ala)_6$	3.7	0.8	−4.7	7.6	3.9 ± 0.2	−0.2 ± 0.2
$(Aib)_{10}$	3.9	3.9	−13.5	13.5	6.0 ± 0.7	−2.1 ± 0.7
$(Aib)_8$	0.3	2.9	−13.1	10.5	2.0 ± 0.5	−1.7 ± 0.5
$(Aib)_8$	−2.8	1.6	−12.0	7.6	−2.8 ± 0.2	0.0 ± 0.2
			Transition State[c]			
$(Aib)_{10}$	7.0	2.2	−2.4	7.2	9.1 ± 0.6	−2.1 ± 0.6
$(Aib)_8$	3.2	1.3	−2.5	4.4	4.6 ± 0.4	−1.4 ± 0.4
$(Aib)_8$	0.3	0.4	−1.9	1.8	0.5 ± 0.2	−0.2 ± 0.2

[a] All values calculated from free energy profiles, as described in the methods section. For $(Ala)_n$ profiles connect α-helix minima to $(\phi,\psi) = (-60°,-29°)$. For $(Aib)_n$ profiles connect α-helix minima to 3_{10}-helix minima. Statistical errors of the total free energy and the potential energy components were below 0.1 kcal/mol in all cases. Units: kcal/mol. [b] int: internal strain component; elec: electrostatic interaction component; vdW: van der Waals interaction component. [c] Relative to α helix.

The free energy differences between the $(Ala)_n$ α-helix minima and the idealized 3_{10}-helix state at $(\phi,\psi) = (-60°,-29°)$ are 14.2 ± 0.1, 8.3 ± 0.1, and 3.7 ± 0.1 kcal/mol for $(Ala)_n$, n = 10, 8, 6, respectively. Our decaalanine result is in good agreement with the 13.5 kcal/mol obtained using the AMBER/OPLS potential[14] and in qualitative agreement with the 8.0 kcal/mol found in Cedar force field calculations.[19] However, it must be noted that the 3_{10}-helix structure found in the last work was quite different than those in all other simulations and experimental studies, with both ϕ and ψ dihedrals close to −40°.[19]

In our $(Ala)_{10}$ calculations the 3_{10}-helix is disfavored in terms of all energy components—internal strain, electrostatic, and van der Waals. For the shorter helices electrostatic interactions increasingly favor the 3_{10}-helix over the α-helix. For these systems the effect of the presence of the extra hydrogen bond in the 3_{10}-helix is prevalent in the electrostatics, while in the $(Ala)_{10}$ system the fact that the 3_{10}-helix hydrogen bonds are less optimal than in the α-helix predominates (see next section). The energy−entropy decompositions indicate that in the longer helices, n = 8, 10, the 3_{10}-helix state is more disordered than the α-helix, leading to a stabilization of the 3_{10}-helix by about 3 kcal/mol. This is in qualitative agreement with the shapes of the free energy surfaces (Figure 2) and second derivatives (Table 2). An entropic stabilization of the 3_{10}-helix relative to the α-helix in vacuum by about 4 kcal/mol was predicted from a normal mode analysis of $(Ala)_8$[21] and molecular dynamics simulations of $(Ala)_{10}$.[19]

For $(Aib)_n$ the 3_{10}-helix becomes systematically more stable relative to the α-helix with decreasing n, with $\Delta A = A(3_{10}\text{-helix}) - A(\alpha\text{-helix}) = 3.9 \pm 0.1$, 0.3 ± 0.1, and -2.8 ± 0.1 kcal/mol for n = 10, 8, 6, respectively (Table 3). The decrease of ΔA with peptide length in our results is about 1.6−1.8 kcal/mol per residue, and the break-even length, where the α-helix and 3_{10}-helix become equally stable, is close to $n = 8$. These values are in very good agreement with previous vacuum AMBER/OPLS simulations of Marshall *et al.*, which gave ΔA of 3.2 and 1.1 kcal/mol for $(Aib)_{10}$ and $(Aib)_9$, respectively, and a break-even length of 7.5.[15,16] Zhang and Hermans predicted an even stronger propensity of $(Aib)_{10}$ for the 3_{10}-helix structure in vacuum, obtaining $\Delta A = -4.3$ kcal/mol in all-atom and 0.0 kcal/mol in united atom simulations.[19]

The energy decompositions in Table 3 indicate that the 3_{10}-helix exhibits higher internal strain and more unfavorable van der Waals interactions than the α-helix in $(Aib)_n$ systems. However, the 3_{10}-helix is strongly preferred in terms of electrostatic interactions. For shorter helices the unfavorable internal strain and van der Waals contributions become smaller, and the slowly varying favorable electrostatic term dominates ΔA. The electrostatic contributions in $(Aib)_n$ are much larger than in $(Ala)_n$ systems, because of qualitative differences in hydrogen bonding (see next section). As in the case of $(Ala)_n$ systems, the energy−entropy decompositions indicate that for the longer $(Aib)_n$ helices the 3_{10}-helix is more disordered than the α-helix, which stabilizes the 3_{10}-helix by about 2 kcal/mol. This result is in accord with the shapes of the free energy surfaces (Figure 2) and values of second derivatives of the free energy (Table 2). In previous one-dimensional free energy simulations of Aib_{10}, Marshall *et al.* found a similar $-T\Delta S$ contribution of −1.2 kcal/mol,[16] while Zhang and Hermans obtained −4.3 kcal/mol.[19]

The barrier for the hypothetical concerted α-helix → 3_{10}-helix transition was found to be 7.0 ± 0.1, 3.2 ± 0.1, and 0.3 ± 0.1 kcal/mol above the α-helix state for $(Aib)_n$, n = 10, 8, 6, respectively. Marshall *et al.* found 3.3 and 0.8 kcal/mol barriers for the sequential transition in $(Aib)_{10}$ and $(Aib)_9$, respectively.[15,16] It thus appears that the sequential transition should be the favored one; this type of transition was found in unconstrained vacuum[21] and solvated[14] simulations and in a path optimization study.[15] Zhang and Hermans have also reported spontaneous transitions from 3_{10}-helix to α-helix for $(Ala)_{10}$ and from α-helix to 3_{10}-helix for $(Aib)_{10}$ during 15−20 ps unconstrained simulations in vacuum.[19] In our simulations the transition state exhibits unfavorable internal strain and van der Waals energy but is electrostatically stabilized compared to the α-helix.

Molecular Origin of $(Aib)_n$ 3_{10}-Helix Stability. To understand the molecular origin of the increased stability of the 3_{10}-helix in Aib peptides, it is helpful to correlate the free energy changes from Table 3 with the structures of the different helices from Table 4. The molecular dynamics average structures of the α-helices of $(Ala)_n$ and $(Aib)_n$ contained $n - 2$ hydrogen bonds, for n = 6, 8, 10. Out of these hydrogen bonds, $n - 4$ followed the standard α-helix pattern, connecting the peptide C═O of residue i with the peptide N−H of residue $i + 4$; the additional two hydrogen bonds involved the terminal blocking groups. The 3_{10}-helix structures contained $n - 1$ hydrogen bonds; $n - 3$ were i−($i + 3$) bonds typical of the 3_{10}-helix,

TABLE 4: Structural Parameters of Regular $(Ala)_{10}$ and $(Aib)_{10}$ Helices[a]

	helix structure[b]			H-bond geometry[c]			
system	rise Å	turn deg	radius Å	$R_{O...H}$ Å	$R_{O...N}$ Å	⟨(N−H−O), deg	⟨(H−O−C), deg
$(Ala)_{10}$							
α-helix	1.50	99.4	2.24	2.08	3.03	161.1	148.0
3_{10}-helix	1.93	109.2	1.84	2.25	3.17	156.8	121.8
$(Aib)_{10}$							
α-helix	1.58	96.9	2.34	2.26	3.24	170.8	155.9
3_{10}-helix	2.02	113.9	1.82	2.16	3.13	161.3	131.2

[a] All structures were obtained as averages from 40 ps molecular dynamics with fixed (ϕ,ψ) at 300 K. $(Ala)_{10}$: $(\phi,\psi) = (-65.8°,-40.8°)$ for α-helix and $(-60°,-29°)$ for 3_{10}-helix. $(Aib)_{10}$: $(\phi,\psi) = (-56.8°,-51.6°)$ for α-helix and $(-53.2°,-29.7°)$ for 3_{10}-helix. [b] Helix axes were determined using the algorithm of ref 41. The helix rise is the average distance between projections of consecutive C_α positions on the helix axis; the helix turn is the average angle between lines perpendicular to helix axis passing through consecutive C_α atoms; the helix radius is the root-mean-square distance of the C_α atoms from the axis. [c] $(C{=}O)_i...(H-N)_{i+4}$ hydrogen bonds for α-helices, $(C{=}O)_i...(H-N)_{i+3}$ for 3_{10}-helices; *i* is the residue number.

and two involved terminal blocking groups. As expected, the 3_{10} helices contained one extra helical hydrogen bond than the α-helices in each case.

The $(Ala)_{10}$ α-helix structure with a rise of 1.50 Å and turn of 99.4° is very close to the "ideal" structure (rise 1.50 Å and turn 100°[17]). Upon transition to the 3_{10}-helix, the rise increases by about 0.4 Å, the turn increases by 10°, and the helix radius decreases by 0.4 Å. These structural changes lead to greater internal strain and unfavorable van der Waals interactions in the 3_{10}-helix (Table 3). Although the 3_{10}-helix has one more hydrogen bond than the α-helix, the 3_{10}-helix hydrogen bonds are weaker, as seen in their increased length and larger deviations from the linear arrangement (Table 4). As a result, the $(Ala)_{10}$ 3_{10}-helix has overall less favorable electrostatic interactions (Table 3). It is interesting that in the shorter peptides, for which the fractional increase in the number of hydrogen bonds upon α-helix → 3_{10}-helix transition is greater, the electrostatic contribution has the opposite sign.

As the result of methylation, the $(Aib)_{10}$ α-helix structure has a rise of 1.58 Å and turn of 96.9°, which is further away from the ideal α-helix than the $(Ala)_{10}$ structure. The $(Aib)_{10}$ α-helix hydrogen bonds are about 0.1 Å longer than those in the $(Ala)_{10}$ α-helix. The methylation thus appears to destabilize the α-helix structure. The structural changes upon transition to the 3_{10}-helix in $(Aib)_{10}$ are similar to those found in $(Ala)_{10}$: the rise increases by about 0.4 Å, the turn increases by 7°, and the helix radius decreases by 0.5 Å. Due to the presence of the extra methyl groups, this structural change leads to more internal strain and more unfavorable van der Waals interactions in $(Aib)_{10}$ than in the case of $(Ala)_{10}$ (see Table 3). However, for $(Aib)_{10}$ the 3_{10}-helix exhibits shorter hydrogen bonds than the α-helix. The improved hydrogen bond geometry and the increased number of hydrogen bonds in the $(Aib)_{10}$ 3_{10}-helix structure lead to its significant electrostatic stabilization relative to the α-helix. The presence of the additional α-methyl groups in $(Aib)_{10}$ thus induces structural changes that electrostatically stabilize the the 3_{10}-helix relative to the α-helix, leading to the increased propensity of Aib-containing peptides for the 3_{10}-helix structure, in agreement with experimental observations.[16,39,40] In the tightly packed $(Aib)_n$ 3_{10}-helices the large unfavorable van der Waals contribution falls off quickly with the number of residues *n* (Table 3). However, the effect of improved hydrogen bonding in the $(Aib)_n$ 3_{10}-helix relative to the α-helix becomes more pronounced for smaller *n* (e.g. the $(Aib)_8$ 3_{10}-helix hydrogen bonds are shorter than the α-helix ones by almost 0.2 Å). This leads to a relatively small variation of the electrostatic contribution to ΔA with *n*. As a result, for *n* below 8 the electrostatic effects dominate, and the 3_{10}-helix becomes the most stable form for $(Aib)_n$ peptides.

It is interesting to compare our results with previous vacuum simulations of $(Aib)_{10}$ by Marshall *et al.*[16] The overall 3_{10}-helix−α-helix free energy difference, ΔA, and the energy−entropy decompositions, ΔU, $-T\Delta S$, obtained in that work were quite similar to our results (see previous section). The energy term decompositions were also qualitatively similar. Our simulations predict a van der Waals term of 13.5 kcal/mol and an electrostatic one of −13.5 kcal/mol, while Marshall *et al.* obtained 17.7 and −5.0 kcal/mol, respectively.[16] Also, the average (ϕ,ψ) values of the α-helix, $(-59°,-50°)$, and 3_{10}-helix, $(-57°,-26°)$ of ref 16 are quite similar to ours (Table 1). However, there is one qualitative disagreement—in contrast to our results, Marshall *et al.* find that the hydrogen bonds are longer in the $(Aib)_{10}$ 3_{10}-helix than in the α-helix. This is reflected in the lower electrostatic ΔA component obtained by these authors. There are a number of differences between simulation protocols used in our study and in the previous $(Aib)_{10}$ simulations:[16] we used the CHARMM all-atom model with 12 Å nonbonded cutoff, regular helix structures, and thermodynamic integration, while Marshall *et al.* employed the AMBER/OPLS extended atom model with an 8 Å cutoff, irregular structures obtained from molecular dynamics with only the end-to-end distance constraint, and umbrella sampling. In spite of these differences, the two studies gave results similar in a number of aspects. It is difficult to determine which of the protocol differences is responsible for the one discrepancy.

In contrast to our results, Zhang and Hermans obtained significantly stronger stabilization of the $(Aib)_{10}$ 3_{10}-helix relative to the α-helix in vacuum, with a free energy difference of −4.3 kcal/mol in all-atom and 0.0 kcal/mol in united atom simulations.[19] In this case the differences may be traced not only to different molecular models and simulation protocols but also to different structures predicted for the 3_{10}-helix state. While our regular free energy minimum structures fell within the experimentally observed range, those of Zhang and Hermans were markedly different.[19] Interestingly, Zhang and Hermans' analysis of the source of the 3_{10}-helix stability in Aib peptides is qualitatively similar to ours—they identified a destabilization of the state by repulsion between methyl groups.

V. Conclusions

Vacuum free energy surfaces for regular helical states of $(Ala)_n$ and $(Aib)_n$ homopeptides, $n = 6, 8, 10$, have been explored using the new multidimensional conformational integration approach. Two-dimensional free energy gradient and free energy maps were generated in $\phi-\psi$ space to visualize variation of free energy with conformation in the studied systems. For $(Ala)_n$ α-helical minima were found for $n = 6, 8, 10$ and a π-helical minimum for $n = 10$, while all studied $(Aib)_n$ peptides had both α- and 3_{10}-helical stable states. The locations of the free energy minima were roughly determined from free energy maps and were refined by the novel procedure of free

energy optimization by steepest descent down the gradient, leading to structures in excellent agreement with experimental data for both $(Ala)_n$ and $(Aib)_n$. The stability of the minima with respect to deformations was studied by calculating numerical free energy second derivatives and diagonalizing the matrix of second derivatives of the free energy surface. As expected, the stability decreased with peptide length for all structures. Also, the 3_{10}-helices were systematically easier to deform than the corresponding α-helices.

Free energy differences between the α- and 3_{10}-helical states were determined by integrating the gradient along connecting paths. For $(Ala)_n$ the α-helix was the most stable state in the studied conformational region. For $(Aib)_n$ the α-helix was more stable for $n = 10$ and the 3_{10}-helix for $n = 6$; at $n = 8$ the free energies of the two structures were approximately equal. Analysis of free energy components and molecular structures revealed the molecular mechanism for the propensity of Aib peptides for the 3_{10}-helix structure in the interplay between the quality and quantity of hydrogen bonds. The $(Ala)_{10}$ α-helix was favored over the 3_{10}-helix by all energy terms, exhibiting lower internal strain, lower van der Waals repulsion, and more favorable electrostatic interactions. Although the 3_{10}-helix has one more hydrogen bond, in $(Ala)_n$ each individual helical hydrogen bond is weaker in the 3_{10}-helix than in the α-helix. In $(Aib)_n$ peptides the added bulk of the α-methyls subtly deforms the helices, inducing larger internal strain and larger van der Waals repulsion than in corresponding $(Ala)_n$ structures and making the $(Aib)_n$ hydrogen bond geometry better in the 3_{10}- than in the α-helix. The synergistic effect of greater number of hydrogen bonds and improved interactions within each bond leads to strong electrostatic stabilization of the $(Aib)_n$ 3_{10}-helix, making it the favored structure for short peptides.

The results obtained using the new CFTI approach were generally in good agreement with previous simulations of the same or related systems. Moreover, the CFTI method enabled generation of several types of new valuable information on multidimensional free energy surfaces of flexible molecules. Free energy gradient maps provided a powerful way of visualizing the variation of free energy with conformation. The free energy optimization method described here is a completely new approach to locating molecular stable states. Calculation of second derivatives of the free energy is also a novel way of describing the stability of free energy minima with respect to small deformations. The free energy decomposition analysis enables generation of useful physicochemical insights into the simulated phenomena. Additionally, free energy simulations in which all soft degrees of freedom are constrained tend to converge very quickly, effectively overcoming the conformational sampling problem. Applications of these powerful features of the CFTI approach to study more complicated systems by including solvent and considering irregular structures and larger, more complex molecules are already under way.

Acknowledgment. The authors thank Professor Martin Karplus for making available CHARMM version 22 parameters prior to publication and the Kansas Institute for Theoretical and Computational Science and Molecular Graphics and Modeling Laboratory at the University of Kansas for use of computer resources. This work was supported by the Petroleum Research Fund of the American Chemical Society (Grant 29566-G4), by a K*STAR EPSCoR FIRST Award, and by the University of Kansas General Research Fund.

References and Notes

(1) Mezei, M.; Beveridge, D. L. *Ann. N. Y. Acad. Sci.* **1986**, *482*, 1−23.
(2) Beveridge, D. L.; DiCapua, F. M. *Annu. Rev. Biophys. Biophys. Chem.* **1989**, *18*, 431−492.
(3) Straatsma, T. P.; McCammon, J. A. *Annu. Rev. Phys. Chem.* **1992**, *43*, 407−435.
(4) Elber, R. *Curr. Opin. Struct. Biol.* **1996**, *6*, 232−235.
(5) Brooks, C. L., III; Case, David A. *Chem. Rev.* **1993**, *93*, 2487−2502.
(6) Kuczera, K.; Gao, J.; Tidor, B.; Karplus, M. *Proc. Natl. Acad. Sci. U.S.A.* **1990**, *87*, 8481−8485.
(7) Gao, J.; Kuczera, K.; Tidor, B.; Karplus, M. *Science* **1989**, *244*, 1069−1072.
(8) Kuczera, K. *J. Comput. Chem.* **1996**, *17*, 1726−1749.
(9) Straatsma, T. P.; McCammon, J. A. *J. Chem. Phys.* **1991**, *95*, 1175−1188.
(10) Smith, D. E.; Haymet, A. D. J. *J. Chem. Phys.* **1993**, *98*, 6445−6454.
(11) Kaminski, G.; Duffy, E. M.; Matsui, T.; Jorgensen, W. L. *J. Phys. Chem.* **1994**, *98*, 13077−13082.
(12) Smith, P. E.; Pettitt, B. M. *Biopolymers* **1992**, *32*, 1623−1629.
(13) Boczko, E. M.; Brooks, C. L., III. *Science* **1995**, *269*, 393−396.
(14) Tirado-Rives, J.; Maxwell, D. S.; Jorgensen, W. L. *J. Am. Chem. Soc.* **1993**, *115*, 11590−11593.
(15) Huston, S. E.; Marshall, G. E. *Biopolymers* **1994**, *34*, 75−90.
(16) Smythe, M. L.; Huston, S. E.; Marshall, G. E. *J. Am. Chem. Soc.* **1995**, *117*, 5445−5452.
(17) Creighton, T. E. *Proteins. Structures and Molecular Properties;* W. H. Freeman: New York**,** 1993.
(18) Hermans, J. *Curr. Opin. Struct. Biol.* **1993**, *3*, 270−276.
(19) Zhang, L.; Hermans, J. *J. Am. Chem. Soc.* **1994**, *116*, 11915−11921.
(20) Barlow, D. J.; Thornton, J. M. J. *J. Mol. Biol.* **1988**, *201*, 601−619.
(21) Basu, G.; Hirata, F.; Go, N. *J. Am. Chem. Soc.* **1994**, *116*, 6307−6315.
(22) Pratt, L. R.; Hsu, C. S.; Chandler, D. *J. Chem. Phys.* **1978**, *68*, 4202−4212.
(23) Carter, E. A.; Ciccotti, G.; Hynes, J. T.; Kapral, R. *Chem. Phys. Lett.* **1989**, *156*, 472−477.
(24) Kuczera, K. *Biopolymers* **1996**, *39*, 221−242.
(25) Brooks, B. R.; Bruccoleri, R.; Olafson, B.; States, D.; Swaminathan, S.; Karplus, M. *J. Comput. Chem.* **1983**, *4*, 187−217.
(26) MacKerell, A. D., Jr.; Field, M.; Fischer, S.; Watanabe, M.; Karplus, M. Manuscript in preparation.
(27) MacKerell, A. D., Jr.; Wiorkiewicz-Kuczera, J.; Karplus, M. *J. Am. Chem. Soc.* **1995**, *117*, 11946−11975.
(28) Loncharich, R. J.; Brooks, B. R. *Proteins* **1989**, *6*, 32−45.
(29) Tobias, D. J.; Brooks, C. L., III. *J. Chem. Phys.* **1988**, *89*, 5115−5127.
(30) Tobias, D. J.; Brooks, C. L., III. *J. Chem. Phys.* **1990**, *92*, 2582−2592.
(31) Press, W. H.; Flannery, B. P.; Teukolsky, S. A.; Vetterling, W. T. *Numerical Recipes: The Art of Scientific Computing*; Cambridge University Press: Cambridge, 1986.
(32) Schlick, T. Optimization methods in computational chemistry. In *Reviews in Computational Chemistry*; Lipkowitz, K. B., Boyd, D. B., Eds., VCH: New York, 1992; Vol. 3.
(33) Bevington, P. R. *Data Reduction and Error Analysis for the Physical Sciences*, 2nd ed.; McGraw-Hill: New York, 1992.
(34) Brooks, C. L., III; Karplus, M.; Petitt, B. M. *Proteins: A Theoretical Perspective of Dynamics, Structure, and Thermodynamics*; John Wiley and Sons: New York, 1988.
(35) Chotia, C. *Annu. Rev. Biochem.* **1984**, *53*, 537−572.
(36) Marshall, G. R.; Beusen, D. D. Structural basis of peptide channel formation. In *Biomembrane electrochemistry*; Blank, M., Vodyanoy, I., Eds.; American Chemical Society: Washington, DC**,** 1994; pp 259−314.
(37) Karle, I. L.; Flippen-Andersen, J.; Uma, K.; Balaram, P. *Curr. Sci.* **1990**, *59*, 875−885.
(38) Bavioso, A.; Benedetti, E.; DiBlasio, B.; Pavone, V.; Pedone, C.; Toniolo, C.; Bonora, G. M. *Proc. Natl. Acad. Sci. U.S.A.* **1986**, *83*, 1988−1992.
(39) Pavone, V.; Di, B. B.; Santini, A.; Benedetti, E.; Pedone, C.; Toniolo, C.; Crisma, M. *J. Mol. Biol.* **1990**, *214*, 633−635.
(40) Otoda, K.; Yasuyuki, K.; Kimura, S.; Imanishi, Y. *Biopolymers* **1993**, *33*, 1337−1345.
(41) Aqvist, J. *Comput. Chem.* **1986**, *10*, 97−99.